

Cross Attention Based Style Distribution for Controllable Person Image Synthesis

Xinyue Zhou¹, Mingyu Yin¹, Xinyuan Chen³, Li Sun^{1,2*}, Changxin Gao⁴, and Qingli Li¹

¹Shanghai Key Laboratory of Multidimensional Information Processing,
²Key Laboratory of Advanced Theory and Application in Statistics and Data Science,
 East China Normal University, Shanghai, China
³Shanghai AI Laboratory, Shanghai, China
⁴Huazhong University of Science and Technology, Wuhan, China



Fig. 1. Left: given the source image and target pose, our model is able to transfer the pose and generate the target parsing map as required. Note that we have only a single training stage without independent generation for the target parsing map. However, our model still synthesizes it precisely by cross attention based style distribution module. Right: Our model also enables virtual try-on and head(identity) swapping by explicitly controlling the poses and per-body-part appearance of source and reference images.

Abstract. Controllable person image synthesis task enables a wide range of applications through explicit control over body pose and appearance. In this paper, we propose a cross attention based style distribution module that computes between the source semantic styles and target pose for pose transfer. The module intentionally selects the style represented by each semantic and distributes them according to the target pose. The attention matrix in cross attention expresses the dynamic similarities between the target pose and the source styles for all semantics. Therefore, it can be utilized to route the color and texture from the source

* Corresponding author, email: sunli@ee.ecnu.edu.cn.

image, and is further constrained by the target parsing map to achieve a clearer objective. At the same time, to encode the source appearance accurately, the self attention among different semantic styles is also added. The effectiveness of our model is validated quantitatively and qualitatively on pose transfer and virtual try-on tasks. Codes are available at <https://github.com/xyzhouo/CASD>.

Keywords: Person image synthesis, Pose transfer, Virtual try-on

1 Introduction

Synthesizing realistic person images under explicit control of the body pose and appearance has many potential applications, such as person reID [47,38,6], video generation [40,16] and virtual clothes try-on [9,34,3,7], *etc.* Recently, the conditional GAN is employed to transfer the source style into the specified target pose. The generator connects the intended style with the required pose in its different layers. *E.g.*, PATN [50], HPT [41], ADGAN [23] insert several repeated modules with the same structure to combine style and pose features. However, these modules are usually composed of common operations, such as Squeeze-and-Excitation (SE) [11] or Adaptive Instance Normalization (AdaIN) [12], which lacks the ability to align source style with target pose.

In contrast, the 2D or 3D deformation is applied in the task with a clearer motivation. DefGAN [28], GFLA [26] and Intr-Flow [15] estimate the correspondence between the source and target pose to guide the spread of appearance features. Although these methods generate realistic texture, they may produce noticeable artifacts when faced with large deformations. Besides, more than one training stages are often needed, and the unreliable flow from the first stage limits the quality of results.

This paper aims for the better fusion on features of both source image and target pose in a single training stage. Instead of directly estimating the geometry deformation and warping source features to fulfill target pose, we propose a simple cross attention based style distribution (CASD) module to calculate between the target pose and the source style represented by each semantic, and distribute the source semantic styles to the target pose. The basic idea is to employ the coarse fusion features under target pose as queries, requiring the source styles from different semantic components as keys and values to update and refine them. Following ADGAN [23], appearance within each semantic region is described by a style encoder, which extracts the color and texture within the corresponding region (such as head, arms, or legs, *etc.*). The style features are dynamically distributed by the CASD block for each query position under the target pose. Particularly, values from each semantic are softly weighted and summed together according to the attention matrix, so that they are matched with target pose. The aligned feature can be further utilized to affect the input to the decoder.

To further improve the synthesis quality, we have some special designs within CASD block. First, to tightly link styles from different semantics, the self atten-

tion is performed among them, making each style no longer independent with others. Second, another routing scheme, in the same size with attention matrix, is also employed for style routing. It is directly predicted from the target pose without exhaustive comparisons with keys of styles. Third, extra constraint from target parsing map is incorporated on the attention matrix, so that the attention head has a clearer motivation. In this way, our attention matrix represents the predicted target parsing map. Additionally, our model can also achieve virtual try-on and head(identity) swapping based on reference images by exchanging the specific semantic region in style features. Fig 1 shows some applications of our model. The contributions of the paper can be summarized into following aspects.

- We propose cross attention based style distribution (CASD) module for controllable person image synthesis, which softly selects the source style represented by each semantic and distributes them to the target pose.
- We intentionally add self attention to connect styles from different semantic components, and let the model predict the attention matrix based on the target pose. Moreover, the target parsing maps are used as the ground truths for the attention matrix, giving the model an evident object during training.
- We can achieve applications in image manipulation by explicit controlling over body pose and appearance, *e.g.*, pose transfer, parsing map generation, virtual try-on and head(identity) swapping.
- Extensive experiments on DeepFashion dataset validates the effectiveness of our proposed model. Particularly, the synthesis quality has been greatly improved, indicated by both quantitative metrics and user study.

2 Related Work

Human pose transfer is first proposed in [20], and becomes well developed in recent years due to the advancement in image synthesis. Most of the existing works need paired training data, which employ the ground truth under target pose during training. Though a few of them are fully unsupervised [21,5,25,30,44,44,48,27], they are not of our major concern. Previous research can be characterized into either two- (or multi-) stage or one-stage methods. The former first generates coarse images or foreground masks, and then gives them to the second stage generator as input for refinement. In [1], the model first segments the foreground from image into different body components, and then applies learnable spatial deformations on them to generate the foreground image. GFLA [26] pretrains a network to estimate the 2D flow and occlusion mask based on source image, source and target poses. Afterwards, it uses them to warp local patches of the source to match the required pose. Li *et.al.* [15] fit a 3D mesh human model onto the 2D image, and train the first stage model to predict the 3D flow, which is employed to warp the source appearance in the second stage. LiquidGAN [16] also adopts the 3D model to guide the geometry deformation within the foreground region. Although geometry-based methods generate realistic texture, they may fail to extract accurate motions, resulting

in noticeable artifacts. On the other hand, without any deformation operation, PISE [43] and SPGnet [19] synthesize the target parsing maps, given the source masks, source poses and target poses as input in the first stage. Then it generates the image with the help of them in the second stage. These work show that the parsing maps under target pose have potential to be exploited for pose transfer.

Compared to two-stage methods, the single stage model has light training burden. Different from [1], DefGAN [28] explicitly computes the local 2D affine transformation between source and target patches, and applies the deformation to align source features to the target pose. PATN [50] proposes a repeated pose attention module, consisting of the computation like SE-Net, to combine features from the appearance and pose. ADGAN [23] uses a texture encoder to extract style vectors within each semantic, and gives them to several AdaIN residual blocks to synthesize the target image. XingGAN [31] proposes two types of cross attention blocks to fuse features from the target pose and source appearance in two directions, repeatedly. Although these models design the fusion block of pose and appearance style, they lack the operation to align source appearance with the target pose. CoCosNet [44,48] computes the dense correspondences between cross-domain images by attention-based operation. However, each target position is only related to a local patch of the source image, which implies that the correlation matrix should be a sparse matrix, and the dense correlation matrix leads to quadratic memory consumption. Our model deals with this problem by an efficient CASD block.

Attention and transformer modules first appear in NLP [33], which enlarge the receptive field in a dynamic way. Non-local network [36] is its first attempt in image domain. The scheme becomes increasingly popular in various tasks including image classification [4,32,17,35], object detection [2,49] and semantic segmentation [13,46] due to its effectiveness. There are basically two different ways for it which are self and cross attention. Self attention projects the queries, keys and values from the same token set, while cross attention usually obtains keys and values from one set, and queries from another one. The computation process then becomes the same, measuring the similarity between queries and keys to form an attention matrix, which is used to weight values to update query tokens. Based on the repeated attention module, multi-stage transformer can be built. Note that adding the MLP (FFN) and residual connection between stages are crucial and become a designing routine, for which we also follows.

3 Method

3.1 Overview Framework

Given a source image I_s under the pose P_s , our goal is to synthesize a high fidelity image \hat{I}_t under a different target pose P_t . \hat{I}_t should not only fulfil the pose requirement, but also have the same appearance with I_s . Fig 2 shows the overview of the proposed generation model. It consists of a pose encoder E_p , a semantic region style encoder E_s and a decoder Dec . Besides, there are several cross attention based style distribution (CASD) blocks which are the key

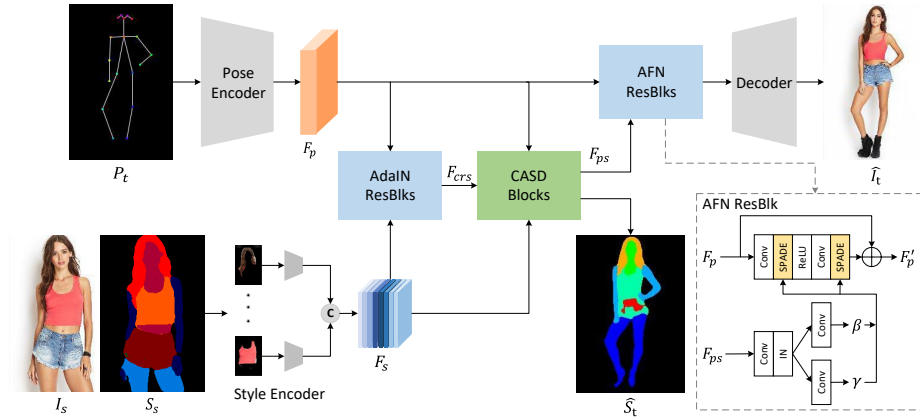


Fig. 2. Overview architecture of our proposed generator. There are separate pose and style encoders, with their outputs F_p and F_s being fused by AdaIN ResBlks and Cross Attention based Style Distribution (CASD) blocks, and giving the pose-aligned feature F_{ps} as the output. Then, the same F_{ps} is adapted to decoder through AFN ResBlks. The key component, CASD Block, consists of both self and cross attention, and can also output the predicted target parsing maps \hat{S}_t .

components in our generator. Before and after the attention, there are several AdaIN residual blocks and Aligned Feature Normalization (AFN) residual blocks with the similar design as [24,42]. The former coarsely adapts the source style to the target pose, while the latter incorporates the pose-aligned feature from the CASD blocks into the decoder. Both of them are learnable, which change the feature statistics in their affecting layers.

As is shown in Fig 2, the desired P_t is directly used as the input by encoder E_p , which describes the key point positions of human body. For each point, we make a single channel heatmap with a predefined standard deviation to describe its location. Except the individual point, we additionally adopt straight lines between selected points to better model the pose structure. There are totally 18 points and 12 lines, so $P_t \in \mathbb{R}^{H \times W \times 30}$. To facilitate accurate style extraction from I_s , we follow the strategy in [23], which employs the source parsing map $S_s \in \mathbb{R}^{H \times W \times N_s}$ to separate the full image into regions, so that E_s independently encodes the styles in different semantics. N_s is the total number of semantics in the parsing map. During training, the ground truth image I_t and its corresponding parsing map S_t are exploited. Note that $F_p \in \mathbb{R}^{H \times W \times C}$ and $F_s \in \mathbb{R}^{N_s \times 1 \times 1 \times C}$ represent the pose and style features from E_p and E_s , respectively. They are utilized by the CASD blocks, whose details are introduced in the following section. Moreover, the CASD block is repeated by multiple times, *e.g.* twice, gradually completing the fusion between F_p and F_s , and forming a better aligned feature F_{ps} . Finally, F_{ps} is given to AFN from the side branch to take its effect. Besides, our CASD block can also output the predicted target parsing map \hat{S}_t by constraining the cross attention matrix.

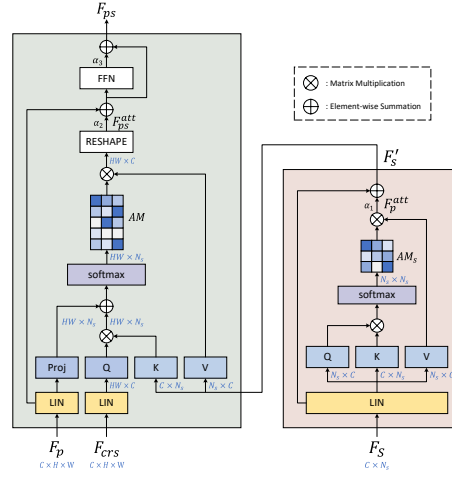


Fig. 3. Illustrations of the cross attention based style distribution (CASD) block. On the right, self attention is performed on the source style features F_s , giving the updated F'_s as the output. On the left, cross attention is computed between the coarsely aligned feature F_{crs} and the updated style feature F'_s . The pose F_p also joins the cross attention. And by constraining the cross attention matrix AM , predicted target parsing maps \hat{S}_t is generated. Note that α_{1-3} indicates the learnable scaling factors.

3.2 Pre- and Post-Attention Style injection

Since the source style $F_s^i \in \mathbb{R}^{1 \times 1 \times C}$ is independently encoded by a shared-weight encoder E_s , where $i = 1, 2, \dots, N_s$ is the semantic index, they may not appropriate for style injection together. So we first combine F_s^i from different semantic regions through an MLP, and give results to AdaIN ResBlks to roughly combine F_s with F_p , specifying the coarse fusion F_{crs} reflecting the target pose P_t , which then participates cross attention as queries in the CASD blocks.

After the CASD blocks, we have F_{ps} which is obviously superior to F_{crs} , and is suitable for the utilization by Dec . Instead of giving F_{ps} directly to Dec , we design an AFN ResBlks to employ it as a conditional feature. Within the block, an offset β and a scaling factor γ are first predicted. Then, they take effect through AFN, which performs the conditional normalization according to β and γ . Note that F_{ps} , β and γ are in the same size.

3.3 Cross Attention based Style Distribution Block

The computation in CASD block includes two stages, which are self attention and cross attention stages, as is depicted in Fig 3. The two types of attention are carried out in sequence, and they together align the source style F_s according to the target pose feature F_p . We describe them in the following two sections.

Self attention for Style Features The self attention is performed among F_s^i , so that each F_s^i of a particular semantic is connected with others F_s^j where $j \neq i$. We simplify the classic design on self attention module in transformer [33]. Traditionally, there are three learnable projection heads W_Q , W_K and W_V , and they are in the same shape $W_Q, W_K, W_V \in \mathbb{R}^{C \times C}$. These heads are responsible for mapping the input tokens F_s into the query Q , key K and value V . In our application, to reduce learnable parameters, we omit W_Q and W_K , and directly use F_s as both query and key. However, we keep W_V and it yields $V \in \mathbb{R}^{N_s \times C}$ in the same dimension of F_s . The self attention, computing the update style feature F_s^{att} , can be summarized into Eq (1).

$$\begin{aligned} F_s^{att} &= \text{Attention}(Q, K, V) = \text{Softmax}(QK^T/\sqrt{C})V \\ Q &= F_s, \quad K = F_s, \quad V = F_s W_V \end{aligned} \quad (1)$$

Here the attention module essentially compares the similarities of different semantic styles, so that each F_s^i in F_s absorbs information from other style tokens F_s^j . Note that we also follow the common designs in transformer. Particularly, there is a residual connection between F_s and F_s^{att} , so they are added, and given to later layers. The final style is denoted by F'_s , as is shown on the right of Fig 3. Moreover, different from traditional transformer, we employ Layer Instance Normalization (SW-LIN) proposed in [39] to replace LN for better synthesis.

Cross Attention The cross attention module further adapts the source style F'_s into the required pose, shown on the left of Fig 3. Such attention is carried out across different domains, between the coarse fusion F_{crs} output from AdaIN resblks and the style feature F'_s . Therefore, different from the previous self attention, its result F_{ps} has spatial dimensions, and actually reflects how to distribute the source style under an intended pose. In this module, F_{crs} from AdaIN ResBlks is treated as queries Q . Specifically, there are totally $H \times W$ unique queries. Each of them is a C -dim vector. F'_s provides the keys K for comparison with Q and values V for soft selection.

Here we aggregate the common attention computation as is shown in Eq (2). $F_{ps}^{att} \in \mathbb{R}^{H \times W \times C}$ is the updated amount on query after the attention, in the same size with F_{crs} .

$$\begin{aligned} F_{ps}^{att} &= \text{Attention}(Q, F_p, K, V) = AM \cdot V \\ &= \left(\text{Softmax} \left(\frac{QK^T}{\sqrt{C}} + \text{Proj}(F_p) \right) \right) V \end{aligned} \quad (2)$$

Note that we set $Q = F_{crs} W_Q$, $K = F'_s W_K$ and $V = F'_s W_V$, so the attention actually combines the features F_{crs} with source styles F'_s . In Eq (2), the first term in the bracket indicates the regular attention matrix which exhaustively computes the similarity between every Q - K pair. It is of the shape $H \times W \times N_s$ and determines the possible belonging semantic for each position. Since there are projection heads W_Q and W_K to adjust query and key, the attention matrix is fully dynamic, which is harmful to model convergence. Our solution is to add the

second term with the same shape as the first one, forming the augmented attention matrix AM , and let it participate value routing. $\text{Proj}(\cdot)$ is a linear projection head which directly outputs a routing scheme based only on F_p . Therefore, it implies that the model is able to predict the target parsing map for each position, given the encoded pose feature F_p . Some recent works like SPGNet [19] or PISE [43] has a separate training stage to generate the target parsing map according to the required pose. Our model has a similar intention, but it is more convenient with only a single training stage. In the following section, we add a constraint on the attention matrix to generate the predicted target parsing map.

After the cross attention in Eq (2), we follow the routine in transformer, which first makes the element-wise summation between F_{ps}^{att} and F_p , then gives the result to an FFN, leading to a better pose feature F_{ps} which combines the source style for the next stage.

3.4 Learning Objectives

Similar to the previous method [50,23], we employ the adversarial loss L_{adv} , reconstruction loss L_{rec} , perceptual loss L_{perc} and contextual loss L_{CX} as our learning objectives. Additionally, we also adopt an attention matrix cross-entropy loss L_{AMCE} and an LPIPS loss L_{LPIPS} to train our model. The full learning objectives are formulated in Eq (3),

$$L_{full} = \lambda_{adv}L_{adv} + \lambda_{rec}L_{rec} + \lambda_{perc}L_{perc} + \lambda_{CX}L_{CX} + \lambda_{AMCE}L_{AMCE} + \lambda_{LPIPS}L_{LPIPS} \quad (3)$$

where λ_{adv} , λ_{rec} , λ_{perc} , λ_{CX} , λ_{AMCE} and λ_{LPIPS} are hyper-parameters controlling the relative importance of these objectives. They are detailed as follows.

Attention Matrix Cross-entropy Loss. To train our model with an evident object, we adopt cross-entropy loss to constrain the attention matrix AM close to target parsing map S_t , which is defined as:

$$L_{AMCE} = - \sum_{i=1}^H \sum_{j=1}^W \sum_{c=1}^{N_s} S_t(i, j, c) \log(AM(i, j, c)). \quad (4)$$

where i, j denote the position of spatial dimension in the attention matrix AM , and c denotes the position of semantic dimension in attention matrix AM . By employing this loss in the training process, our model can generate the predicted target parsing map in a single stage.

Adversarial loss. We adopt a pose discriminator D_p and a style discriminator D_s to help G generate more realistic result in adversarial training. Specifically, real pose pairs (P_t, I_t) and fake pose pairs (P_t, \hat{I}_t) are feed into D_p for pose consistency. Meanwhile, real image pairs (I_s, I_t) and fake image pairs (I_s, \hat{I}_t) are feed into D_s for style consistency. Note that both discriminators are trained with G in an end-to-end way to promote each other.

$$L_{adv} = \mathbb{E}_{I_s, I_t, P_t} [\log(D_s(I_s, I_t) \cdot D_p(P_t, I_t))] + \mathbb{E}_{I_s, P_t} [\log(1 - D_s(I_s, G(I_s, P_t))) \cdot (1 - D_p(P_t, G(I_s, P_t)))] \quad (5)$$

Reconstruction and perceptual loss. The reconstruction loss L_{rec} is used to encourage the generated image \hat{I}_t to be similar with ground-truth I_t at the pixel level, which is computed as $L_{rec} = \|\hat{I}_t - I_t\|_1$. The perceptual loss calculates the L_1 distance between the features extracted from the pre-trained VGG-19 network [29]. It can be written as $L_{perc} = \sum_i \|\phi_i(\hat{I}_t) - \phi_i(I_t)\|_1$, where ϕ_i is the feature map of the i -th layer of the pre-trained VGG-19 network.

Contextual Loss. We also adopt contextual loss, which is first proposed in [22], aiming to measure the similarity between two non-aligned images for image transformation. It is computed in Eq (6).

$$L_{CX} = -\log\left(CX\left(F^l(\hat{I}_t), F^l(I_t)\right)\right) \quad (6)$$

Here $F^l(\hat{I}_t)$ and $F^l(I_t)$ denotes the feature extracted from layer $l = \text{relu}\{3.2, 4.2\}$ of the pre-trained VGG-19 for images \hat{I}_t and I_t , respectively, and CX denotes the cosine similarity metric between features.

LPIPS Loss. In order to reduce distortions and learn perceptual similarities, we integrate the LPIPS loss [45], which has been shown to better preserve image quality compared to the more standard perceptual loss:

$$L_{LPIPS} = \|F(\hat{I}_t) - F(I_t)\|_2 \quad (7)$$

where $F(\cdot)$ denotes the perceptual feature extracted from pre-trained VGG-16 network.

4 Experiments

4.1 Experimental Setup

Dataset. We carry out experiments on DeepFashion (In-shop Clothes Retrieval Benchmark) [18], which contains 52,712 high-quality person images with the resolution of 256×256 . Following the same data configuration in [50], we split this dataset into training and testing subsets with 101,966 and 8,570 pairs, respectively. Additionally, we use the segmentation masks obtained from the human parser [8]. Note that the person ID of the training and testing sets do not overlap.

Evaluation Metrics. We employ four metrics SSIM [37], FID [10], LPIPS [45] and PSNR for evaluation. Peak Signal to Noise Ratio (PSNR) and Structural Similarity Index Measure (SSIM) is the most commonly used in image generation task with known ground truths. The former utilizes the mean square error to give an overall evaluation, while the latter calculates the global variance and mean to assess the structural similarity. Meanwhile, Learned Perceptual Image Patch Similarity (LPIPS) is another metric to compute the distance between the generations and ground truths in the perceptual domain. Besides, Fréchet Inception Distance (FID) is employed to measure the realism of the generated images. It calculates the Wasserstein-2 distance between the distributions of the generated and real data.

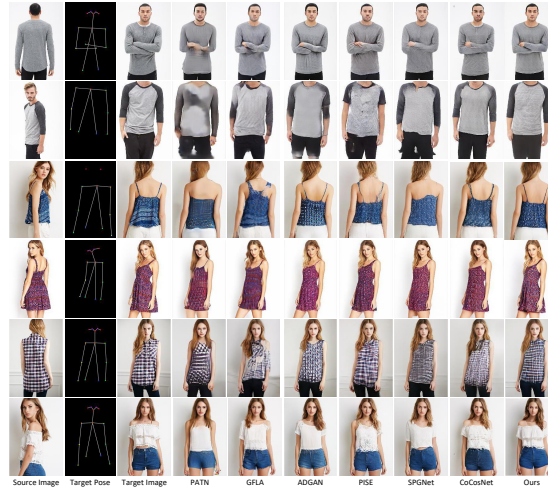


Fig. 4. Qualitative comparison between our method and other state-of-the-arts. The target ground truths and the synthesized results from each models are listed in rows.

Implementation Details. Our method is implemented in PyTorch and trained 2 NVIDIA Tesla-A100 GPUs with the batch size being equal to 16. We adopt Adam optimizer [14] with $\beta_1 = 0.5$, $\beta_2 = 0.999$ to train our model for around 330k iterations, using the same epochs with other works [23]. The weights of the learning objectives are set as: $\lambda_{AMCE} = 0.1$, $\lambda_{LPIPS} = 1$, $\lambda_{rec} = 1$, $\lambda_{perc} = 1$, $\lambda_{adv} = 5$ and $\lambda_{CX} = 0.1$, without tuning. The number of semantic part is $N_s = 8$, which includes the ordinary semantics as background, pants, hair, glove, face, dress, arms and legs. Furthermore, the learning rate is initially set to 0.001, and linearly decayed to 0 after 115k iterations. Following above configuration, we alternatively optimize the generator and two discriminators. We train our model for pose transfer task as described in Sec 3, after the convergence of training, we use the same trained model for all tasks, *e.g.*, pose transfer, virtual try-on, head(identity) swapping and parsing map generation.

4.2 Pose Transfer

In this section, we compare our method with several state-of-the-art methods, including PATN [50], GFLA [26], ADGAN [23], PISE [43], SPGNet [19] and CoCosNet [44]. Quantitative and qualitative results as well as user study are conducted to verify the effectiveness of our method. All the results are obtained by directly using the source code and well-trained models published by their authors. Since CoCosNet uses a different train/test split, we directly uses its well-trained model on our test set.

Quantitative comparison. The quantitative results are listed in Table 1. Notably, our method achieves the best performance on most metrics compared with the other methods, which can be attributed to the proposed CASD block.

Table 1. Comparisons on metrics for image quality and user study. SSIM, FID, LPIPS and PSNR are the quantitative metrics for synthesized images. R2G, G2R and Jab are metrics computed from users’ feedback.

Models	SSIM \uparrow	FID \downarrow	LPIPS \downarrow	PSNR \uparrow	R2G \uparrow	G2R \uparrow	Jab \uparrow
PATN [50]	0.6709	20.7509	0.2562	31.14	19.14	31.78	0.26%
GFLA [26]	0.7074	10.5730	0.2341	31.42	19.53	35.07	13.72%
ADGAN [23]	0.6721	14.4580	0.2283	31.28	23.49	38.67	11.17%
PISE [43]	0.6629	13.6100	0.2059	31.33	-	-	14.89%
SPGNet [19]	0.6770	12.2430	0.2105	31.22	19.47	36.80	17.26%
CoCosNet [44]	0.6746	14.6742	0.2437	31.07	-	-	13.73%
Ours	0.7248	11.3732	0.1936	31.67	24.67	40.52	28.96%

Qualitative comparison. In Fig 9, we compare the generated results from different methods. It can be observed that our method produces more realistic and reasonable results (*e.g.*, the second, third and penultimate rows). More importantly, our model can well retain the details from the source image (*e.g.*, the fourth and last rows). Moreover, even if target pose is complex (*e.g.*, the first row), our method can still generate it precisely.

User study. While both quantitative and qualitative comparisons can evaluate the performance of the generated results in different aspects, human pose transfer tasks tend to be user-oriented. Therefore, we conduct a user study with 30 volunteers to evaluate the performance in terms of human perception. The user study consists of two parts. (*i*) Comparison with ground-truths. Following [19], we randomly select 30 real images and 30 generated images from test set and shuffle them. Volunteers are required to determine whether a given image is real or fake within a second. (*ii*) Comparison with the other methods, we present volunteers 30 random selected image pairs that include source image, target pose, ground-truth and images generated by our method and baselines. Volunteers are asked to select the most realistic and reasonable image with respect to the source image and ground truth. Note that we shuffle all the generated images for fairness. The results are shown in the right part of Table 1. Here we adopt three metrics, namely **R2G**: the percentage of the real images treated as the generated images; **G2R**: the percentage of the generated images treated as real images; **Jab**: the percentage of images judged to be the best among all models. Higher values of these three metrics mean better performance. We can observe that our model achieves the best results, especially about 11% higher than the 2-nd best one on Jab.

4.3 Ablation Study

In this section, we perform ablation study to further verify our assumptions and evaluate the contribution of each component in our model. We implement 3 variants by alternatively removing a specific component from the full model (w/o self-attn, w/o AM_p , w/o L_{AMCE}).



Fig. 5. The qualitative results of ablation study. The ground truths and the synthesized images from each ablation model are listed in columns.

Table 2. Quantitative ablations on each proposed component in the full model. The performances of the final model are given the last row. In the above three rows, we intentionally exclude one component from the full model. Details are given in Sec 4.3.

Model	SSIM \uparrow	FID \downarrow	LPIPS \downarrow	PSNR \uparrow
w/o self-attn	0.7201	13.2462	0.2017	31.52
w/o AM_p	0.7213	12.4265	0.1985	31.48
w/o L_{AMCE}	0.7156	14.7513	0.2126	31.41
Ours-Full	0.7248	11.3732	0.1936	31.67

W/o self-attn. This model removes self attention in CASD blocks, only uses cross attention, which directly feeds F_s into cross attention as Key and Value.

W/o AM_p . The model removes $AM_p = \text{Proj}(Q)$ in CASD blocks in Eq (2), which will not let the model predict the attention matrix based on the target pose.

W/o L_{AMCE} . The model does not adopt L_{AMCE} loss defined in Eq (4) for training, so it can not be explicitly guided by the target parsing map during cross attention.

Full model. It includes all components and achieves the best performance on all quantitative metrics, as is shown Table 5. Meanwhile, it also gives the best visual results as is shown in Fig 10. It's shown that by removing any parts of our proposed model would lead to a performance drop.



Fig. 6. The visual comparisons with other state-of-the-art methods on virtual try-on.

Table 3. Comparisons of the FID score and user study with other state-of-the-art methods on virtual try-on and head(identity) swapping tasks.

Method	Upper Cloth		Pants		Head	
	FID↓	Jab↑	FID↓	Jab↑	FID↓	Jab↑
ADGAN	14.3720	24.67%	14.4446	29.67%	14.4596	23.58%
PISE	14.0537	22.92%	14.2874	22.25%	14.3647	30.75%
Ours	12.5376	52.41%	12.5456	48.08%	12.6578	45.67%

4.4 Virtual Try-on and Head Swapping

Benefiting from the semantic region style encoder, our model can also achieve controllable person image synthesis based on reference images by exchanging the channel feature of specific semantic region in the style features (*e.g.*, upper-body transfer, lower-body transfer and head swapping) without further training. We compare our method with ADGAN [23] and PISE [43]. The visual comparisons are shown in Fig 6. We observe that our model can reconstruct target part and retain other remaining parts more faithfully. In addition, when transferring the lower-body, PISE cannot transfer the target pants to the source person, it will retain the shape of the source person’s pants and only transfer the texture.

For more comprehensive comparisons, quantitative comparison and user study are also conducted. The results are shown in Table 6. In the user study, we randomly select 40 results generated by our method and the other compared methods for each task, and then we invite 30 volunteers to select the most realistic results. **Jab** is the percentage of images judged to be the best among all methods.

Table 4. Comparison of per-class IoU with SPGNet on the predicted target parsing maps.

Model	pants	hair	gloves	face	u-clothes	arms	legs	Bkg	Avg
SPGNet [19]	42.18	66.51	9.36	62.46	67.87	58.46	44.13	84.65	61.89
Ours	49.02	65.87	5.50	67.24	76.72	59.90	50.81	90.28	66.34



Fig. 7. Failure cases caused by incomprehensible garment (left) or pose (right).

4.5 Target parsing map synthesis

Moreover, to intuitively understand of our CASD blocks, we further show the predicted target parsing maps in Fig 1. It shows when given the source image and various target poses, our model can not only transfer the poses, but also synthesize the target parsing maps, though we do not separately build a model to do this. We list the Intersection over Union (IoU) metric between predictions from our method and [8] for all semantics in Table 4. For major semantics, we achieve higher IoU than SPGNet [19]. Note that our model gives the final synthesis images and target parsing map in one stage. The synthesized paired data can be used as training data for segmentation.

5 Limitations

Although our method produces impressive results in most cases, it still fails to generate incomprehensible garments and poses. As shown in Fig 7, a specific knot on a blouse fails to generate and a person in a rare pose can not be synthesized seamlessly. We believe that training the model with more various images will alleviate this problem.

6 Conclusion

This paper presents a cross attention based style distribution block for a single-stage controllable person image synthesis task, which has strong ability to align the source semantic styles with the target poses. The cross attention based style distribution block mainly consists of self and cross attention, which not only captures the source semantic styles accurately, but also aligns them to the target pose precisely. To achieve a clearer objective, the AMCE loss is proposed to constrain the attention matrix in cross attention by target parsing map. Extensive experiments and ablation studies show the satisfactory performance of our model, and the effectiveness of its components. Finally, we show that our model can be easily applied to virtual try-on and head(identity) swapping tasks.

Acknowledgements

This work is supported by the Science and Technology Commission of Shanghai Municipality No.19511120800, Natural Science Foundation of China No.61302125 and No.62102150, and ECNU Multifunctional Platform for Innovation(001).

References

1. Balakrishnan, G., Zhao, A., Dalca, A.V., Durand, F., Gutttag, J.: Synthesizing images of humans in unseen poses. In: Proceedings of the IEEE Conference on Computer Vision and Pattern Recognition. pp. 8340–8348 (2018) [3](#), [4](#)
2. Carion, N., Massa, F., Synnaeve, G., Usunier, N., Kirillov, A., Zagoruyko, S.: End-to-end object detection with transformers. In: European Conference on Computer Vision. pp. 213–229. Springer (2020) [4](#)
3. Dong, H., Liang, X., Shen, X., Wu, B., Chen, B.C., Yin, J.: Fw-gan: Flow-navigated warping gan for video virtual try-on. In: Proceedings of the IEEE/CVF International Conference on Computer Vision. pp. 1161–1170 (2019) [2](#)
4. Dosovitskiy, A., Beyer, L., Kolesnikov, A., Weissenborn, D., Zhai, X., Unterthiner, T., Dehghani, M., Minderer, M., Heigold, G., Gelly, S., et al.: An image is worth 16x16 words: Transformers for image recognition at scale. arXiv preprint arXiv:2010.11929 (2020) [4](#)
5. Esser, P., Sutter, E., Ommer, B.: A variational u-net for conditional appearance and shape generation. In: Proceedings of the IEEE Conference on Computer Vision and Pattern Recognition. pp. 8857–8866 (2018) [3](#)
6. Ge, Y., Li, Z., Zhao, H., Yin, G., Yi, S., Wang, X., Li, H.: Fd-gan: Pose-guided feature distilling gan for robust person re-identification. arXiv preprint arXiv:1810.02936 (2018) [2](#)
7. Ge, Y., Song, Y., Zhang, R., Ge, C., Liu, W., Luo, P.: Parser-free virtual try-on via distilling appearance flows. In: Proceedings of the IEEE/CVF Conference on Computer Vision and Pattern Recognition. pp. 8485–8493 (2021) [2](#)
8. Gong, K., Liang, X., Zhang, D., Shen, X., Lin, L.: Look into person: Self-supervised structure-sensitive learning and a new benchmark for human parsing. In: Proceedings of the IEEE Conference on Computer Vision and Pattern Recognition. pp. 932–940 (2017) [9](#), [14](#)
9. Han, X., Wu, Z., Wu, Z., Yu, R., Davis, L.S.: Viton: An image-based virtual try-on network. In: Proceedings of the IEEE conference on computer vision and pattern recognition. pp. 7543–7552 (2018) [2](#)
10. Heusel, M., Ramsauer, H., Unterthiner, T., Nessler, B., Hochreiter, S.: Gans trained by a two time-scale update rule converge to a local nash equilibrium. *Advances in neural information processing systems* **30** (2017) [9](#)
11. Hu, J., Shen, L., Sun, G.: Squeeze-and-excitation networks. In: Proceedings of the IEEE conference on computer vision and pattern recognition. pp. 7132–7141 (2018) [2](#)
12. Huang, X., Belongie, S.: Arbitrary style transfer in real-time with adaptive instance normalization. In: Proceedings of the IEEE International Conference on Computer Vision. pp. 1501–1510 (2017) [2](#)
13. Huang, Z., Wang, X., Huang, L., Huang, C., Wei, Y., Liu, W.: Ccnet: Criss-cross attention for semantic segmentation. In: Proceedings of the IEEE/CVF International Conference on Computer Vision. pp. 603–612 (2019) [4](#)
14. Kingma, D.P., Ba, J.: Adam: A method for stochastic optimization. arXiv preprint arXiv:1412.6980 (2014) [10](#)
15. Li, Y., Huang, C., Loy, C.C.: Dense intrinsic appearance flow for human pose transfer. In: Proceedings of the IEEE/CVF Conference on Computer Vision and Pattern Recognition. pp. 3693–3702 (2019) [2](#), [3](#)

16. Liu, W., Piao, Z., Min, J., Luo, W., Ma, L., Gao, S.: Liquid warping gan: A unified framework for human motion imitation, appearance transfer and novel view synthesis. In: Proceedings of the IEEE/CVF International Conference on Computer Vision. pp. 5904–5913 (2019) [2](#), [3](#)
17. Liu, Z., Lin, Y., Cao, Y., Hu, H., Wei, Y., Zhang, Z., Lin, S., Guo, B.: Swin transformer: Hierarchical vision transformer using shifted windows. arXiv preprint arXiv:2103.14030 (2021) [4](#)
18. Liu, Z., Luo, P., Qiu, S., Wang, X., Tang, X.: Deepfashion: Powering robust clothes recognition and retrieval with rich annotations. In: Proceedings of IEEE Conference on Computer Vision and Pattern Recognition (CVPR) (June 2016) [9](#)
19. Lv, Z., Li, X., Li, X., Li, F., Lin, T., He, D., Zuo, W.: Learning semantic person image generation by region-adaptive normalization. In: Proceedings of the IEEE/CVF Conference on Computer Vision and Pattern Recognition. pp. 10806–10815 (2021) [4](#), [8](#), [10](#), [11](#), [13](#), [14](#), [19](#)
20. Ma, L., Jia, X., Sun, Q., Schiele, B., Tuytelaars, T., Van Gool, L.: Pose guided person image generation. arXiv preprint arXiv:1705.09368 (2017) [3](#)
21. Ma, L., Sun, Q., Georgoulis, S., Van Gool, L., Schiele, B., Fritz, M.: Disentangled person image generation. In: Proceedings of the IEEE Conference on Computer Vision and Pattern Recognition. pp. 99–108 (2018) [3](#)
22. Mechrez, R., Talmi, I., Zelnik-Manor, L.: The contextual loss for image transformation with non-aligned data. In: Proceedings of the European Conference on Computer Vision (ECCV). pp. 768–783 (2018) [9](#)
23. Men, Y., Mao, Y., Jiang, Y., Ma, W.Y., Lian, Z.: Controllable person image synthesis with attribute-decomposed gan. In: Proceedings of the IEEE/CVF Conference on Computer Vision and Pattern Recognition. pp. 5084–5093 (2020) [2](#), [4](#), [5](#), [8](#), [10](#), [11](#), [13](#), [19](#)
24. Park, T., Liu, M.Y., Wang, T.C., Zhu, J.Y.: Semantic image synthesis with spatially-adaptive normalization. In: Proceedings of the IEEE/CVF Conference on Computer Vision and Pattern Recognition. pp. 2337–2346 (2019) [5](#)
25. Pumarola, A., Agudo, A., Sanfeliu, A., Moreno-Noguer, F.: Unsupervised person image synthesis in arbitrary poses. In: Proceedings of the IEEE Conference on Computer Vision and Pattern Recognition. pp. 8620–8628 (2018) [3](#)
26. Ren, Y., Yu, X., Chen, J., Li, T.H., Li, G.: Deep image spatial transformation for person image generation. In: Proceedings of the IEEE/CVF Conference on Computer Vision and Pattern Recognition. pp. 7690–7699 (2020) [2](#), [3](#), [10](#), [11](#), [19](#)
27. Sanyal, S., Vorobiov, A., Bolkart, T., Loper, M., Mohler, B., Davis, L.S., Romero, J., Black, M.J.: Learning realistic human reposing using cyclic self-supervision with 3d shape, pose, and appearance consistency. In: Proceedings of the IEEE/CVF International Conference on Computer Vision. pp. 11138–11147 (2021) [3](#)
28. Siarohin, A., Sangineto, E., Lathuiliere, S., Sebe, N.: Deformable gans for pose-based human image generation. In: Proceedings of the IEEE Conference on Computer Vision and Pattern Recognition. pp. 3408–3416 (2018) [2](#), [4](#)
29. Simonyan, K., Zisserman, A.: Very deep convolutional networks for large-scale image recognition. arXiv preprint arXiv:1409.1556 (2014) [9](#)
30. Song, S., Zhang, W., Liu, J., Mei, T.: Unsupervised person image generation with semantic parsing transformation. In: Proceedings of the IEEE/CVF Conference on Computer Vision and Pattern Recognition. pp. 2357–2366 (2019) [3](#)
31. Tang, H., Bai, S., Zhang, L., Torr, P.H., Sebe, N.: Xinggan for person image generation. In: European Conference on Computer Vision. pp. 717–734. Springer (2020) [4](#)

32. Touvron, H., Cord, M., Douze, M., Massa, F., Sablayrolles, A., Jégou, H.: Training data-efficient image transformers & distillation through attention. In: International Conference on Machine Learning. pp. 10347–10357. PMLR (2021) [4](#)
33. Vaswani, A., Shazeer, N., Parmar, N., Uszkoreit, J., Jones, L., Gomez, A.N., Kaiser, L., Polosukhin, I.: Attention is all you need. In: Advances in neural information processing systems. pp. 5998–6008 (2017) [4](#), [7](#)
34. Wang, B., Zheng, H., Liang, X., Chen, Y., Lin, L., Yang, M.: Toward characteristic-preserving image-based virtual try-on network. In: Proceedings of the European Conference on Computer Vision (ECCV). pp. 589–604 (2018) [2](#)
35. Wang, W., Xie, E., Li, X., Fan, D.P., Song, K., Liang, D., Lu, T., Luo, P., Shao, L.: Pyramid vision transformer: A versatile backbone for dense prediction without convolutions. arXiv preprint arXiv:2102.12122 (2021) [4](#)
36. Wang, X., Girshick, R., Gupta, A., He, K.: Non-local neural networks. In: Proceedings of the IEEE conference on computer vision and pattern recognition. pp. 7794–7803 (2018) [4](#)
37. Wang, Z., Bovik, A.C., Sheikh, H.R., Simoncelli, E.P.: Image quality assessment: from error visibility to structural similarity. IEEE transactions on image processing **13**(4), 600–612 (2004) [9](#)
38. Wei, L., Zhang, S., Gao, W., Tian, Q.: Person transfer gan to bridge domain gap for person re-identification. In: Proceedings of the IEEE conference on computer vision and pattern recognition. pp. 79–88 (2018) [2](#)
39. Xu, W., Long, C., Wang, R., Wang, G.: Drb-gan: A dynamic resblock generative adversarial network for artistic style transfer. In: Proceedings of the IEEE/CVF International Conference on Computer Vision. pp. 6383–6392 (2021) [7](#)
40. Yang, C., Wang, Z., Zhu, X., Huang, C., Shi, J., Lin, D.: Pose guided human video generation. In: Proceedings of the European Conference on Computer Vision (ECCV). pp. 201–216 (2018) [2](#)
41. Yang, L., Wang, P., Liu, C., Gao, Z., Ren, P., Zhang, X., Wang, S., Ma, S., Hua, X., Gao, W.: Towards fine-grained human pose transfer with detail replenishing network. IEEE Transactions on Image Processing **30**, 2422–2435 (2021) [2](#)
42. Yin, M., Sun, L., Li, Q.: Novel view synthesis on unpaired data by conditional deformable variational auto-encoder. In: European Conference on Computer Vision. pp. 87–103. Springer (2020) [5](#)
43. Zhang, J., Li, K., Lai, Y.K., Yang, J.: Pise: Person image synthesis and editing with decoupled gan. In: Proceedings of the IEEE/CVF Conference on Computer Vision and Pattern Recognition. pp. 7982–7990 (2021) [4](#), [8](#), [10](#), [11](#), [13](#), [19](#)
44. Zhang, P., Zhang, B., Chen, D., Yuan, L., Wen, F.: Cross-domain correspondence learning for exemplar-based image translation. In: Proceedings of the IEEE/CVF Conference on Computer Vision and Pattern Recognition. pp. 5143–5153 (2020) [3](#), [4](#), [10](#), [11](#), [19](#)
45. Zhang, R., Isola, P., Efros, A.A., Shechtman, E., Wang, O.: The unreasonable effectiveness of deep features as a perceptual metric. In: Proceedings of the IEEE conference on computer vision and pattern recognition. pp. 586–595 (2018) [9](#)
46. Zheng, S., Lu, J., Zhao, H., Zhu, X., Luo, Z., Wang, Y., Fu, Y., Feng, J., Xiang, T., Torr, P.H., et al.: Rethinking semantic segmentation from a sequence-to-sequence perspective with transformers. In: Proceedings of the IEEE/CVF Conference on Computer Vision and Pattern Recognition. pp. 6881–6890 (2021) [4](#)
47. Zheng, Z., Zheng, L., Yang, Y.: Unlabeled samples generated by gan improve the person re-identification baseline in vitro. In: Proceedings of the IEEE international conference on computer vision. pp. 3754–3762 (2017) [2](#)

48. Zhou, X., Zhang, B., Zhang, T., Zhang, P., Bao, J., Chen, D., Zhang, Z., Wen, F.: Cocosnet v2: Full-resolution correspondence learning for image translation. In: Proceedings of the IEEE/CVF Conference on Computer Vision and Pattern Recognition. pp. 11465–11475 (2021) [3](#), [4](#)
49. Zhu, X., Su, W., Lu, L., Li, B., Wang, X., Dai, J.: Deformable detr: Deformable transformers for end-to-end object detection. arXiv preprint arXiv:2010.04159 (2020) [4](#)
50. Zhu, Z., Huang, T., Shi, B., Yu, M., Wang, B., Bai, X.: Progressive pose attention transfer for person image generation. In: Proceedings of the IEEE/CVF Conference on Computer Vision and Pattern Recognition. pp. 2347–2356 (2019) [2](#), [4](#), [8](#), [9](#), [10](#), [11](#), [19](#)

Appendix

A Network architectures

In this section, we provide the details of network structure. Table 5, 6, are the network structures of the encoder E, the generator G, respectively. In Conv and Residual Block, F, K and S respectively represent the output dimension, convolution kernel size and stride. IN and LN represent instance normalization and layer normalization, respectively.

B Comparisons with the state-of-the-arts

In Fig 8, We provide additional qualitative comparisons between our method and other state-of-the-arts(*e.g.* PATN [50], GFLA [26], ADGAN [23], PISE [43], SPGNet [19], CoCosNet [44]). Results show that our method can generate more consistent appearance and pose with the target.

C Visualization of the generated parsing maps

We also provide more visualization results of the generated parsing maps in Fig 9. It is clear that cross attention matrix can accurately predict the target parsing map regardless of diverse pose and viewpoint changes, revealing the effectiveness of the proposed cross attention based style distribution module.

D Results of virtual try-on

By exchanging the channel feature of specific semantic region in the style features, our model can achieve virtual try-on task. Additional examples of virtual try-on are shown in Fig 10.

Table 5. The structure of encoder E. In E, we put I_s^i into Pre-trained VGG19 network and take the features of the corresponding layers as side branches, then concat them together with the main branch. Note that we only show one source style I_s^i as an example, where $i = 1, 2, \dots, 8$ is the semantic index. And all I_s^i concat together lastly.

Input	I_s^i ($256 \times 176 \times 3$)
Intermediate Layers	Conv(F = 64, K = 7, S = 1), ReLU
	Concat(Pre – trained VGG19 conv1.1)
	Conv(F = 128, K = 4, S = 2), ReLU
	Concat(Pre – trained VGG19 conv2.1)
	Conv(F = 256, K = 4, S = 2), ReLU
	Concat(Pre – trained VGG19 conv3.1)
	Conv(F = 512, K = 4, S = 2), ReLU
	Concat(Pre – trained VGG19 conv4.1)
	Avg Pooling
	Conv(F = 256, K = 1, S = 1)
Output	F_s^i ($1 \times 1 \times 256$)

Table 6. The structure of the generator G. In AdaIN ResBlocks and AFN ResBlocks, the content in bracket is used as side branch to affect the main branch.

Input	P_t ($256 \times 176 \times 30$)	F_s ($1 \times 1 \times 2048$)
Intermediate Layers	Conv(F = 64, K = 7, S = 1), IN, ReLU	Fc(2048), ReLU
	Conv(F = 128, K = 4, S = 2), IN, ReLU	Fc(256), ReLU
	Conv(F = 256, K = 4, S = 2), IN, ReLU	Fc(256), ReLU
	$F_p = \text{Residual Blocks}(F = 256, K = 3, S = 1) \times 8$	$F_{s'} = \text{Fc}(8192), \text{ReLU}$
	$F_{crs} = \text{AdaIN ResBlock}(F_{s'})$	
	$F_{ps} = \text{CASD}(F_{crs}, F_p, F_s)$	
	$F_{ps} = \text{CASD}(F_{ps}, F_p, F_s)$	
	$F_{p'} = \text{AFN ResBlocks}(F_{ps})$	
	UpSample(scale.factor = 2)	
	Conv(F = 128, K = 5, S = 1), LN, ReLU	
UpSample(scale.factor = 2)		
Conv(F = 64, K = 5, S = 1), LN, ReLU		
Conv(F = 3, K = 7, S = 1), Tanh		
Output	\hat{I}_t ($256 \times 176 \times 3$)	

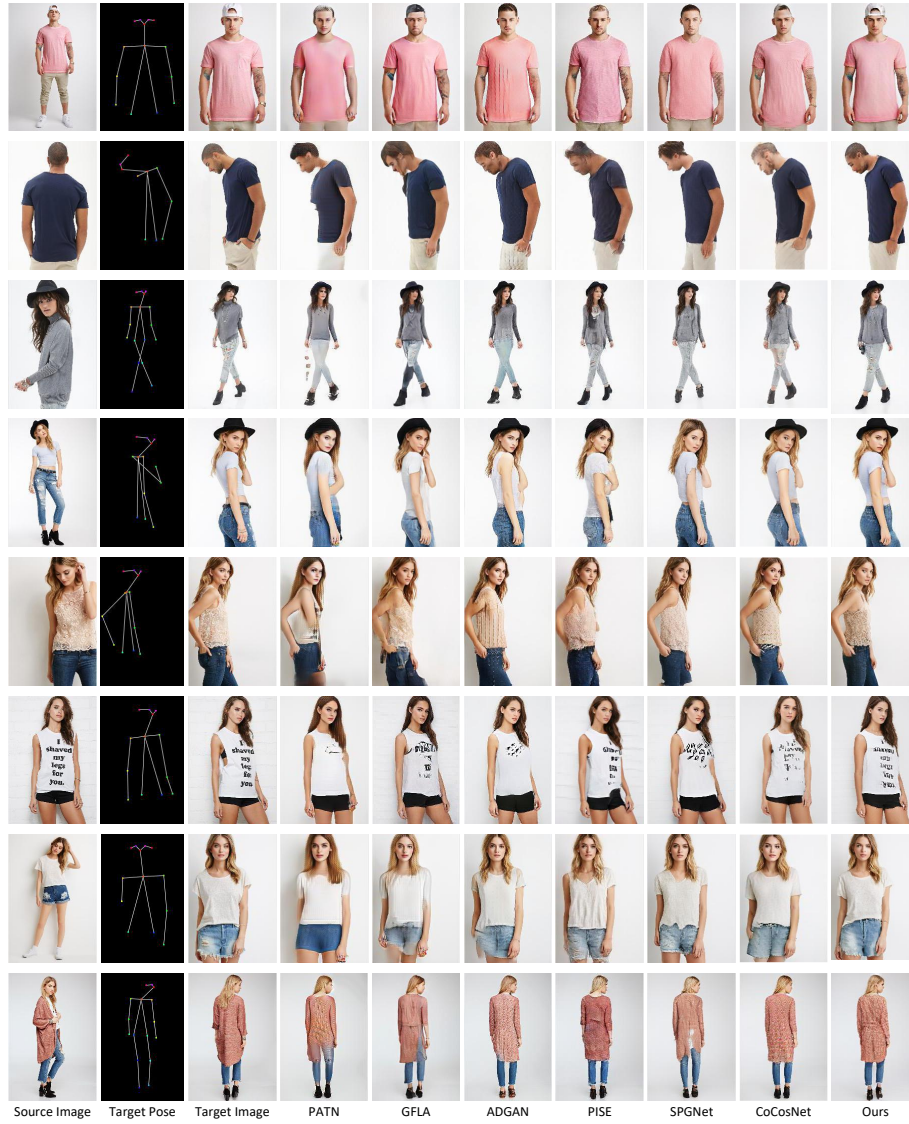


Fig. 8. Qualitative comparison between our method and other state-of-the-arts. The target ground truths and the synthesized results from each models are listed in rows.

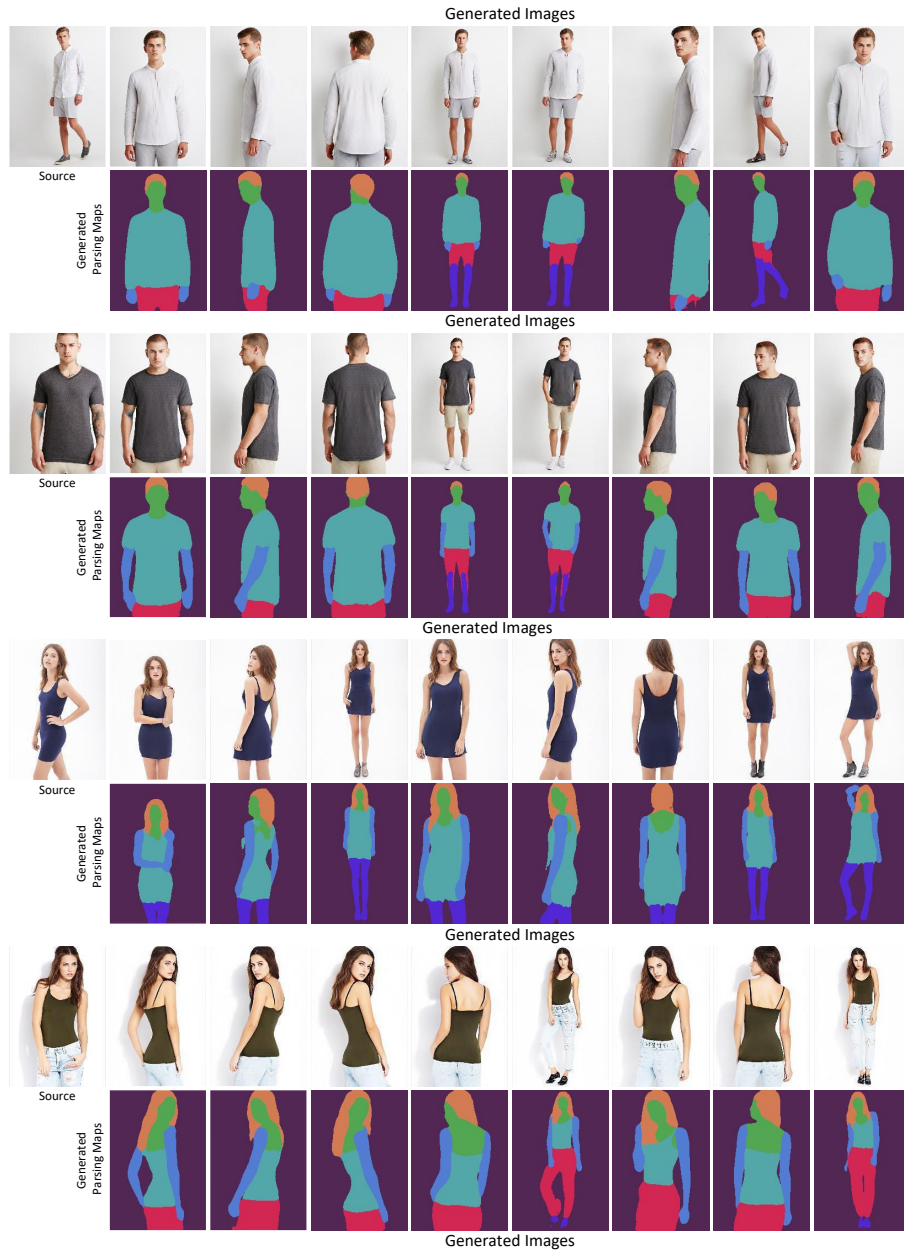


Fig. 9. Given the source image, our model is able to transfer the pose as required. The synthesized person and visualization of the generated target parsing maps are shown.

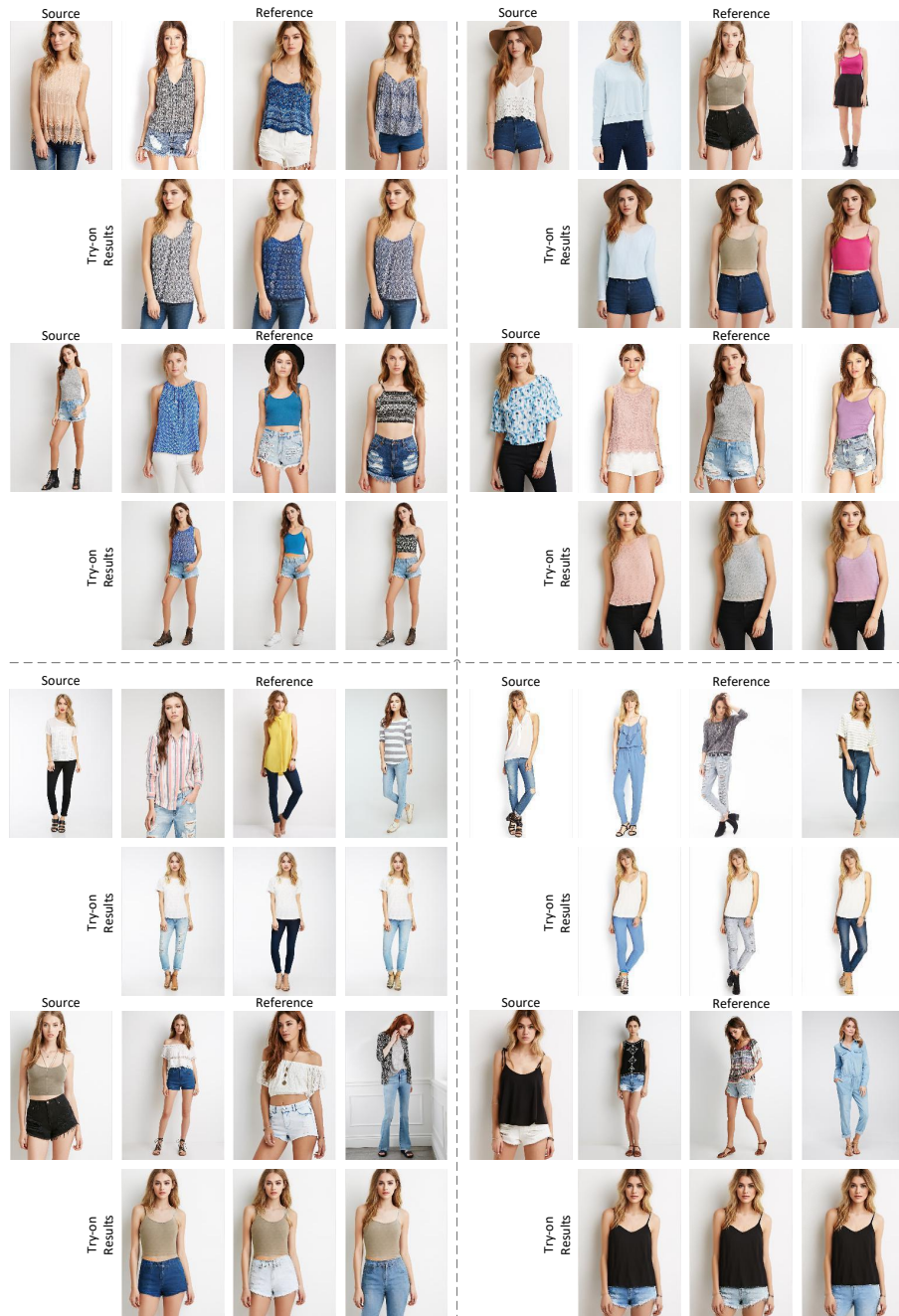


Fig. 10. Given the source image and reference images, our model is able to perform virtual try-on task. The top half is the results of trying on the upper-clothes and the bottom half is the results of trying on the pants.